Journal of Visualization, Vol. 1, No. 1 (1998) 65-77

Simultaneous Planar Velocity Measurements and OH Imaging in a Transverse Jet Flame

Hasselbrink, E.F.*, Mungal, M.G.*, and Hanson, R.K.*

* Department of Mechanical Engineering, Stanford University, Stanford, California 94305, U.S.A.

Received 8 August 1997.
Revised 17 December 1997.

***Abstract*:** We present simultaneous planar velocity and OH fluorescence measurements at the base of a lifted, nonpremixed, transverse methane jet flame of Reynolds number 6300 and jet-to-crossflow velocity ratio 11.5. Velocity measurements are obtained using particle image velocimetry (PIV), while nonresonant OH fluorescence is imaged via excitation of the A←X (1,0) band near 283 nm. It is shown that at the flame base, the regions in the PIV images where particle density drops due to heat release closely overlap the regions where OH appears. Other preliminary results show that the base of the flame sheet typically resides just above a region where velocity magnitude is locally low, about three times the laminar flame speed, and that the fluid accelerates suddenly through the flame base. Experimental issues such as PIV accuracy and OH imaging in the presence of PIV particles are discussed.

***Keywords*:** particle image velocimetry, laser-induced fluorescence, turbulent combustion.

1. Introduction

Particle image velocimetry (PIV) is a mature technique (Lourenco et al., 1989; Adrian,1991) now being applied in combustion flowfields. Recent work has measured the velocity field of a Bunsen burner (Mungal et al., 1995), the velocity at the base of lifted jet flames (Muñiz & Mungal, 1996; Muñiz & Mungal, 1997), and the strain rate induced by a vortex on a flame (Driscoll et al., 1994). These studies used the particle density to determine the approximate location of the flame front. Although often adequate for this purpose, particle density is at best a low resolution, low signal-to-noise ratio measure of fluid temperature.

Planar Laser-Induced Fluorescence (PLIF) imaging, on the other hand, provides high resolution images of species fluorescence (Hanson et al., 1990). For example, PLIF images of the hydroxyl radical OH in combustion flowfields have been obtained by Seitzman et al. (1990), Johnson et al. (1993), and Clemens & Paul (1995), to visualize radical recombination zones. Images of the CH radical have been obtained by Dibble et al. (1990), Stårner et al. (1992), and Paul & Dec (1994) to visualize fuel consumption zones. Measurement of mixture fraction or temperature from PLIF of natural or introduced molecular tracers has also been demonstrated by McMillin et al. (1994) and Palmer & Hanson (1996).

However, flowfield physics and combustion chemistry in turbulent combustion are coupled. Flame blowout, for example, is a consequence of finite-rate chemistry in competition with a finite-rate supply of cold reactants to the flame. As another example, the overall burning rate in a jet flame is determined by the rate of mixing established by the turbulence, but it has been found by Clemens & Paul (1995) that heat release reduces entrainment rates in the near field of turbulent jets.

In short, neither velocity nor scalar imaging alone can provide direct measurements of certain quantities of

interest in turbulent flames. Examples are (1) the residence time of fluid in reaction zones, which is important for understanding pollution formation, especially NO_x production; (2) changes in the local flowfield caused by heat release, which is fundamental to the understanding of flame kinematics; and (3) strain rate fluctuations in reaction zones, which directly influence flame chemistry, and may explain experimentally observed superequilibrium concentrations of OH in turbulent flames reported by Barlow et al. (1989), Barlow & Chen (1992), and Drake & Pitz (1985). Measuring these quantities directly requires simultaneous imaging of a reaction zone marker and the velocity field.

Several studies involving joint planar velocity and scalar measurements in flames have been performed recently. PIV and OH PLIF were performed separately on a repeatable flame/vortex interaction by Mueller et al. (1995). Simultaneous PLIF of biacetyl and PIV in a simple unsteady flame has been reported by Frank et al. (1996). Simultaneous OH PLIF and PIV measurements in turbulent jet flames were first reported concurrently by Hasselbrink et al. (1997) and Rehm & Clemens (1997).

In this paper, we present initial results of simultaneous PIV and OH PLIF measurements near the base of a lifted transverse jet methane flame. This is a complex three-dimensional flow of practical importance in the design of gas turbines, power plants, and industrial flare stacks; the nonreacting jet has been studied previously using PIV by Gogineni et al. (1995). Our primary goal is to use the technique to clearly demonstrate flow and flame interaction at the base of a lifted flame. We also discuss experimental considerations and accuracy of the simultaneous PIV/OH technique in gas-phase combustion flowfields, and evaluate the validity of using particle density as a marker of the flame front.

2. Experiment Description

2.1 Flow Apparatus

A schematic of the experimental arrangement is shown in Fig. 1. The flow facility is a vertical indraft tunnel operating at 2.0 m/s with a 50 × 50 cm test section and rounded inlet with 2.5:1 contraction ratio. A single honeycomb and a cascade of several screens straightens the flow and reduces the freestream turbulence intensity (measured using a hot-wire) to 0.8% without the use of cross-stream particle seeders, and 1.0% when in use (measured using PIV). The tunnel has a large 50 × 80 × 0.63 cm Pyrex window for viewing the flow on the front side, and a 15 × 15 × 0.95 cm quartz window on the back, mounted in the aluminum walls. The back tunnel wall is comprised of several movable plates so that the viewing area may be easily changed. The interior of the wind tunnel is painted black to reduce reflections.

The natural gas jet (93% CH_4) is injected normal to the crossflow through a 25 cm long tube (6.35 mm OD, 4.8 mm ID, 316 stainless steel), protruding 7 cm into the wind tunnel. The jet tube is located within an annular tube (9.5 mm OD) which serves as a hydrogen pilot. Without the hydrogen pilot, the flame lifts off from the jet exit about 7 cm. The jet exit Reynolds number is 6300, the jet-to-crossflow velocity ratio is 11.5, and the blowing ratio $r \equiv \{(\rho_j u_j)/(\rho_\infty u_\infty)\}^{1/2}$ is 8.5.

Both the jet and crossflow are seeded with 0.3 μm (nominal) alumina (Al_2O_3) particles, using fluidized-bed seeders and cyclones for agglomerate removal. Seeded methane is sent directly to the jet tube, while seeded air is directed through a rake of three (9.5 mm OD) copper tubes spaced 4 cm apart, positioned below the tunnel inlet. Each rake is 30 cm long and has several 0.16 mm holes along its length to distribute the particles evenly throughout the central section of the wind tunnel.

2.2 OH Imaging System

With simultaneous PIV, resonant OH PLIF is impossible due to the overwhelming elastic scattering from the particles. Our pumping strategy is excitation of the $A^2\Sigma^+ \leftarrow X^2\Pi$ (1,0) band of OH near 283 nm, combined with detection of the (1,1) and (0,0) bands near 315 nm. Comparative advantages of this pumping scheme and spectroscopic details are given by Seitzman & Hanson (1993). The overlapping $Q_1(9)$ and $Q_2(8)$ transitions were selected to maximize signal.

The elements of the OH imaging system are shown in Fig. 1, shaded in violet. A Lumonics YM-1200 Nd:YAG laser (10 Hz, 1.0 J/pulse) is frequency-doubled to 532 nm and used to pump a Lumonics HD-500 dye laser, which is frequency-doubled again to 283 nm. Pulse energy of 10 mJ/pulse is realized from the dye laser, but severe losses from several UV-protected aluminum turning mirrors, results in about 4-5 mJ/pulse at the image region. A spherical lens and cylindrical lens form the beam into an expanding sheet, approximately 11 cm tall and

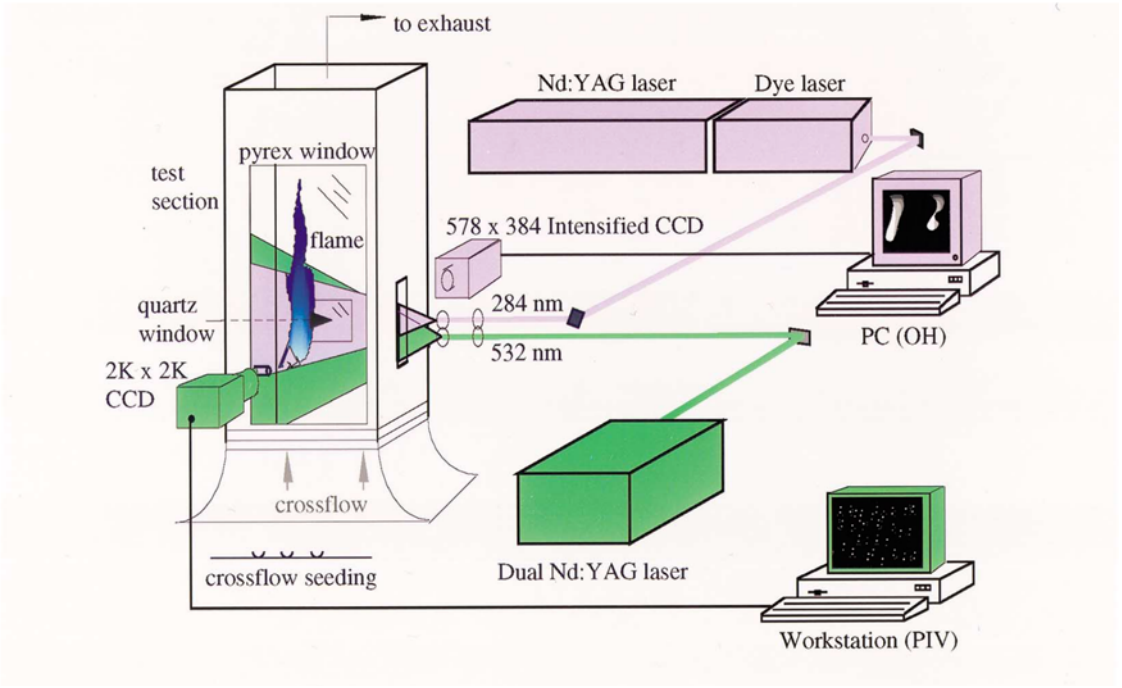

Fig. 1. Schematic of the experimental arrangement for simultaneous OH PLIF and PIV.

500 μm thick at the image region. The fluorescence from naturally occurring OH is captured on a Princeton Instruments 384 × 578 pixel camera with a fiber-coupled MCP intensifier. The camera is equipped with a Nikkor f/4 UV lens, a Schott UG-11 filter to reject flame emission, and three Schott WG-305 filters (1 mm thick) to reject elastic scattering from the particles. Hereafter, this camera will be referred to as the "OH camera", and the Nd:YAG-pumped dye laser system as the "OH laser" to distinguish them from the other laser and camera system in the experiment.

Tuning of the dye laser was performed before each run using a PMT with UG11 and WG-305 filters to record the LIF spectrum around 283 nm from a flat-flame burner. When the laser was tuned off line center, blank images were acquired, ensuring that no soot scattering or broadband fluorescence from other species was observed.

The OH images are qualitative, intended only to visualize the location of flame zones. The only image corrections applied are the subtraction of the mean background level (41 counts, with standard deviation of 2.5 counts — peak signal level is approximately 230 counts). Work performed using this laser concurrently with the present experiments (Kamel et al., 1997) has measured the single-shot beam intensity profile to vary by only 10-15%, so laser sheet intensity corrections are also small enough for visualization purposes. It should be pointed out, however, that quantitative OH imaging is possible in principle. Barlow & Collignon (1991) have found that, although the quenching cross-sections for OH fluorescence varies by about a factor of two across a typical flame, population fraction variations in the $Q_1(6)$ line counter this effect, so that error in interpreting fluorescence signal as OH concentration is less than 20% of the maximum OH concentration across the flame (the error would be greater with the $Q_1(9)$ line used here). However, the PIV particles introduce additional uncertainty of laser sheet extinction by the particles, whose density varies owing to the heat release in the flow. We show later that the magnitude of particle extinction is only about 8% across the viewing region for typical PIV seeding densities, but the extinction before the viewing region presents additional uncertainty.

2.3 PIV Imaging System and Image Processing

The PIV system in this study, shown in Fig. 1 shaded in green, consists of a dual-cavity Nd:YAG laser (Spectra Physics PIV-400, 400 mJ pulse at 532 nm formed into a 250 μm thick sheet), a high resolution CCD camera (2000 × 2000 pixel array, Kodak MegaPlus 4.2 with 105 mm Nikkor lens at f/5.6), and a workstation (IBM RS-6000 Model 370) to process the images. Hereafter, this laser and camera will be referred to as the "PIV laser", and the "PIV camera" to distinguish them from their OH imaging counterparts. Due to timing constraints, the PIV camera

shutter is held open during each run, necessitating the use of a line interference filter (532.0 nm center, 10 nm bandwidth) in front of the camera lens to reject flame emission. As a drawback, however, the filter also rejects 50% of the PIV signal, necessitating the use of +12dB gain in the camera A/D converter. We have also found that some distortion of the particle images occurs with use of the filter, probably resulting from the extreme sensitivity to optical path length in diffraction-limited imaging.

PIV images are processed using the Insight™ software package (originally developed by FFD Inc., now sold by TSI Inc.), which finds the location of the peak in the autocorrelation of a subregion (80 × 80 pixels) of the image as the average particle displacement in that subregion. The imaged area is 49.1 × 49.1 mm, hence each vector represents the average velocity in a 1.96 × 1.96 × 0.25 mm interrogation volume. With 50% interrogation region overlap, a grid of 50 × 50 vectors is obtained. This resolution is coarse, one the order of strained diffusion flame thicknesses, but is chosen for demonstration purposes so that more of the overall jet flow may be captured. Velocity is found by dividing the particle displacement by the time between laser pulses, Δt_{PIV}, which is typically 110 μsec in the present work.

2.4 Experiment Timing and Camera Filtering

The OH laser running at 10Hz is the triggering master for the experiment, necessitated by the fact that beam quality of the dye laser output degrades significantly with deviations from the 10 Hz pulse frequency, probably due to thermal lensing effects in the pump beam. Since the slowest camera (the PIV camera) can only acquire at about 0.6 Hz, only every sixteenth pulse from the OH laser initiates a trigger sequence. Logic electronics ensure that the OH camera has completed its readout before a trigger signal is accepted, and that the intensifier gate can only be opened between the two PIV pulses. Thus the technique is simultaneous inasmuch as the OH image is captured within the same window of time that the PIV image is captured.

Experiment timing and filtering details are shown in Fig. 2. The PIV camera is equipped with a 532 nm line interference filter which rejects all but the PIV laser wavelength. The OH camera is equipped with a Schott UG-11 filter and three cascaded Schott WG-305 filters which reject flame emission and elastic scattering from the particles at 283 nm. The OH camera gate is open for 200 ns during and after the arrival of the OH laser pulse to allow the OH camera to reject flame emmission and view only the OH fluorescence. The OH laser pulse arrives 3 μsec after the first of two PIV laser pulses, and the second PIV pulse arrives another 107 μsec later.

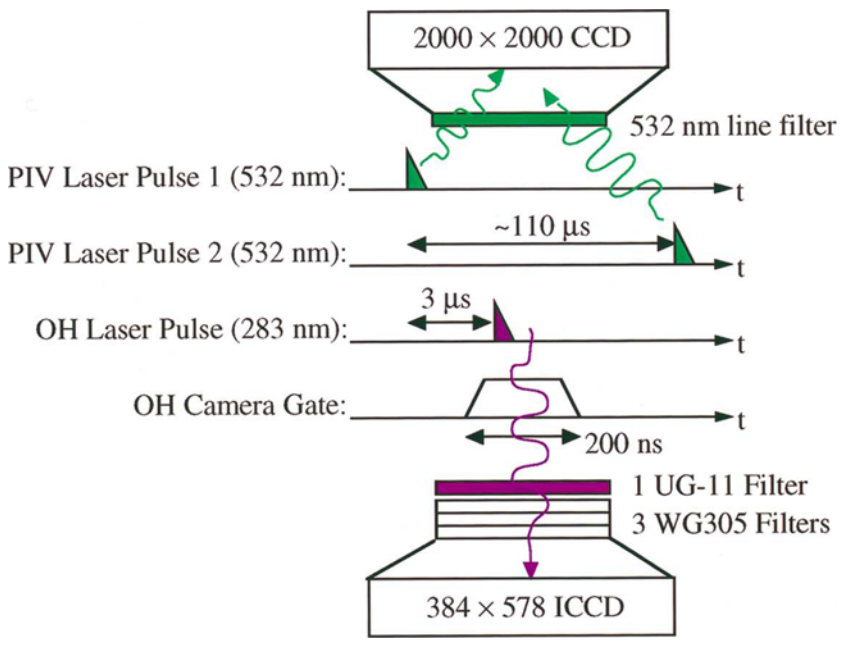

Fig. 2. Timing and optics schematic for the experiment. Temporal arrival of laser pulses into the test section are indicated by colored triangles on the timelines. Light scattering and fluorescence are indicated by wavy lines.

3. Experimental Considerations

3.1 PIV Accuracy

PIV accuracy has been the subject of much previous work (Ashforth-Frost et al., 1993; Westerweel, 1993; Lourenco & Krothapalli, 1995). It is determined by: (1) subpixel resolution, (2) flow/particle velocity differences, and (3) vector dropout and interpolation. We discuss each of these in turn.

Autocorrelation biasing and subpixel resolution has been analyzed in detail by Westerweel (1993), who found that subpixel resolution of the displacement can be at best ±0.1 pixels when using a Gaussian peak estimator. The smallest particle displacements in the flowfield measured were about 5 pixels, so error from subpixel resolution is at best ±2%. When there are strong velocity gradients, autocorrelation PIV measurements are biased towards lower speeds because lower speed particles are more likely to remain in the interrogation region (Keane & Adrian, 1990).

The Stokes number for the present flow is about 0.009, based on a typical particle agglomerate diameter of 1 μm, determined by scanning electron micrographs. This would normally imply that the particles can follow the flow quite accurately. However, significant differences between flow and particle velocities can occur due to thermophoresis, a phenomenon in which a particle experiences a force opposite the direction of the fluid temperature gradient. Thermophoretic diffusivities have been measured directly by Gomez & Rosner (1993), and the effects of thermophoresis on velocity measurements in flames has been studied by Sung et al. (1994), who also give formulae for the thermophoretic velocity (valid for particles smaller than 1 μm diameter). Worst-case thermophoretic velocities (assuming 2000 K/mm temperature gradient at 1300 K, using air properties) in flames are about 15 cm/sec, representing the largest component of systematic error for PIV measurements in flames according to Muñiz et al. (1996), although it can be corrected if the local temperature and temperature gradient are known. Although 15 cm/s may not be a large relative error in the measured velocity in many turbulent flames, it can introduce significant error for derived quantities such as strain rate. For example, in our experiment vectors are spaced 1 mm apart, thus two vectors spaced 2 mm apart are used in a central-differences calculation of one component of the shear rate. If one vector is in the reaction zone and the other one is not, the error due to thermophoresis is (worst case) 75 s^{-1}. A better- resolved experiment with twice our resolution would have an error of up to 150 s^{-1}. This is a significant fraction of the extinction strain rate (about 400 s^{-1}) for methane and propane diffusion flames. As we have no simultaneous temperature measurement, we make no attempt to correct for thermophoresis here, but as we discuss later, simultaneous OH PLIF makes this a possibility.

PIV accuracy is also affected by "dropouts", where in some regions of the flow, a good autocorrelation is not obtained. Often small pockets of dropouts occur due to the presence of an agglomerate, which saturates the CCD array and causes a streak due to "blooming" in the image readout process. Other causes are insufficient particle displacement or out-of-plane motion of the particles in high-turbulence regions. The missing vectors can be interpolated from their neighbors, but the accuracy of their values depends strongly on how many surrounding neighbors were correctly processed. Interpolation over small pockets of dropouts yields results to within a few percent of the actual velocity. This is usually accurate enough for the velocity field, but often not for derived quantities such as vorticity and strain rate.

3.2 OH Imaging in the Presence of Particles

Here we discuss four issues in the OH imaging aspect of the experiment: interpretation of the images, rejection of elastic particle scattering, the magnitude of fluorescence from particle-scattered light, and the possibility of particle/flame interactions.

An important issue with OH imaging in turbulent flows is interpretation of the images. OH formation reactions are fast (~20 μs), but the recombination reactions which eliminate OH are slow (~ 1-5 ms). Hence OH tends to linger in high temperature zones and cannot be considered to be in chemical equilibrium in most turbulent flows. In our case, in the imaged region, $\tau_{flow} = 2$ ms, so that a Damkohler number based on formation reaction rates is $Da_{form} \approx 100$, but based on recombination rates is $Da_{recomb} \approx 1$. Clearly, some care must be exercised in interpreting the OH images. In our favor, however, is the fact that at the base of the flame, the presence of OH usually implies chemical reaction and heat release because OH is initially formed here.

Another important experimental issue is that Mie scattering at the laser wavelength must be rejected by the OH imaging apparatus in the presence of PIV particles. The magnitude of the problem can be estimated by calculating the number of photons per pixel expected from OH and particle scattering. OH signal is estimated

using the fluorescence equation for broad laser line excitation and linear fluorescence,

$$N_{p,\,\mathrm{OH}} = \eta \frac{\Omega}{4\pi} x_{\mathrm{OH}} n V_C f_J(T) \frac{A_{21}}{A_{21}+Q_{21}} B_{12} E_\nu$$

where $\eta\Omega/4\pi$ is the overall collection efficiency, x_{OH} is the OH mole fraction, n the overall number density, V_c the collection volume represented by a pixel, $f_J(T)$ the fraction in the lower state, $A/(A+Q) \approx A/Q$ is the Stern-Vollmer factor or fluorescence yield, B (cm²/J-s) is the transition probability, and E_ν is the spectral fluence of the laser, i.e., the spatial intensity divided by the laser bandwidth (J-Hz^{-1}/cm²). Particle scattering signal can be estimated as

$$N_{p,\,\mathrm{part}} = \eta \frac{\Omega}{4\pi} I Q_{\mathrm{sca}} \pi a_p^2 n_{\mathrm{part}} V_c / h\nu$$

where I is the laser sheet intensity, Q_{sca} is the particle scattering efficiency, a_p is the particle radius, n_{part} is the particle number density, V_c the collection volume of a single pixel, h is the Planck constant and ν the laser frequency. This formulation assumes that all the scattering from a particle falls on a single pixel — actual particle diameter on the CCD array is (in the diffraction limit) $d_t \approx 2.44\lambda(1+M)f\#$ for small particles (Lourenco et al., 1989; Adrian, 1991), smaller than the 23 μm pixels of the OH camera. Typical Q_{sca} for small particles is near two, but may be calculated for small spheres using Mie's approximate formula as given by van de Hulst (1981)

$$Q_{\mathrm{sca}} = 2 - \frac{4}{\rho}\sin\rho + \frac{4}{\rho^2}(1-\cos\rho)$$

where $\rho = 2x(m-1)$, $x = 2\pi a_p/\lambda$, and m is the ratio of particle to fluid index of refraction. This can also be strongly influenced by polarization for particles small compared to the wavelength: the scattering at 90° of incidence is much stronger if the polarization of the beam is in the plane of the laser sheet.

The ratio of OH signal to particle scattering signal,

$$\frac{N_{p,\mathrm{OH}}}{N_{p,\,\mathrm{part}}} = \frac{n\chi_{\mathrm{OH}}}{C_{\mathrm{part}}} f_1(T) \frac{A_{21}}{A_{21}+Q_{21}} \frac{B_{12}h}{Q_{\mathrm{sca}}\pi a_p^2} \frac{\nu}{\Delta\nu}$$

(where $\Delta\nu$ is the laser bandwidth), is independent of collection efficiency, collection volume, and laser intensity. For estimation purposes, we use values for the $Q_1(6)$ line of the $A \leftarrow X$ (1,0) band at 1500 K, as given by Seitzman (1991): $A = 0.88 \times 10^6$ s^{-1}, $Q = 0.7 \times 10^9$ s^{-1}, $B = 9.9 \times 10^{12}$ cm²/J-s, and $f_1 = 0.031$. The laser bandwidth is 15GHz, based on a comparison of our tuning scans with calculated spectra. We assume $m = 2$, $a_p = 1$ μm, and $n_{\mathrm{part}} = 50$ mm^{-3}. Thus the ratio of peak OH fluorescence to typical particle scattering is approximately 1.25×10^{-2}.

To reduce particle scattering signal below the OH signal level, we use cascaded WG-305 colored glass filters. The manufacturer's specifications indicate that each millimeter of thickness of WG-305 glass provides a transmittance of 6×10^{-2} at 283 nm. Thus two 1 mm filters have a transmittance of 0.4% and three filters a transmittance of 0.025%, yielding an expected OH-to-particle signal ratio of about 3 and 50, respectively. A side-by-side comparison in Fig. 3 shows that as expected, two 1 mm WG-305 filters might be adequate for visualization, but that a third greatly improves the OH signal purity. The additional filtering comes at a modest cost to signal — each WG-305 has about 80% transmittance at 315 nm.

Another particle scattering concern is that scattered light might induce significant fluorescence of OH outside of the laser sheet. The magnitude of the scattering relative to the incident beam can be estimated by considering the laser sheet extinction, and assuming (as a worst case) that extinction is due entirely to scattering (no absorption). The extinction of the laser sheet by particles is given by $I/I_o = \exp(-\gamma L)$, where I_o and I are the intensities before and after traversing a distance L, and $\gamma = Q_{\mathrm{sca}} n_{\mathrm{part}} \pi a_p^2$. This formulation does not account for multiple scattering, and is only valid for $\gamma L << 1$. Using the same assumptions as before, for the present experiment $\gamma = 0.0013$ mm^{-1}. Thus, across a 3 mm OH structure, only about 0.5% of the incident beam is scattered, and hence fluorescence from out-of-plane OH is negligible. We note, however, that across the 65 mm wide viewing region, extinction is 8%. This implies that attempts to perform *quantitative* single-pulse PLIF, simultaneous with PIV, may require correction for laser sheet extinction, which also occurs in seeded regions before the viewing region.

It is unlikely that the particles affect the flame reactions or thermal transport in the flow, with the possible exception of radiative losses. Flames in a flow laden with Al_2O_3 particles are significantly brighter and yellower than without, and radiation losses are probably larger. However, the particles survive the flame and do not react, and are much smaller than minimum ignition lengths for any fuel. As for advective transport, mass loading in the

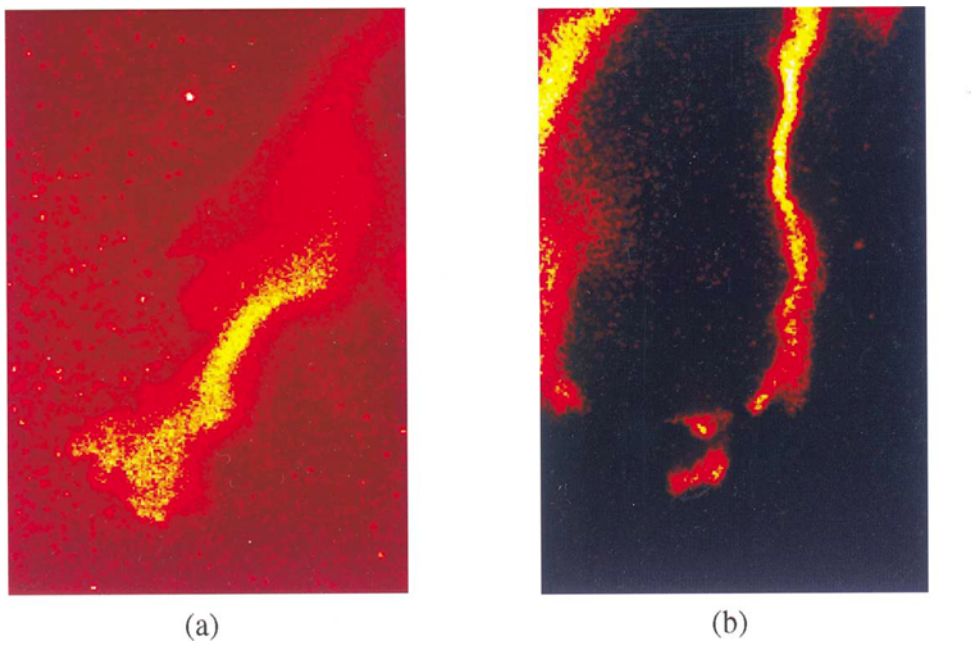

Fig. 3. OH PLIF image in a natural gas jet in the presence of PIV particle seeding, using (a) two 1 mm WG 305 filters to attenuate laser-wavelength particle scattering. (b) Using three WG 305 filters. Both images are presented using the same intensity look-up table.

flowfield is negligible (about 3×10^{-4}), so overall thermal transport by the particles is also quite small. As a further check, we can also consider the 1/e thermal lag time of each particle. Assuming that the particle is approximately isothermal ($Bi << 1$), this time is $\tau_{thermal} = \rho c V/Ah$, where $\rho \approx 3500$ kg/m^3 is the particle density, $c \approx 1000$ J/kg-K its specific heat, V its volume, A its area, and h its average convective heat transfer coefficient. For Stokes flow around a sphere, $Nu_D = hD/k_{fluid} = 2$, so that $\tau_{thermal} = \rho c D^2/12k_{fluid}$; for $D = 1\mu$m, and $k_{fluid} = 0.0672$ W/m-K (air at 1000 K) $\tau_{thermal} = 4$ μs. Therefore particle thermal lag should be negligible even in the fastest reacting zones of the flow.

4. Results

4.1 Particle Density / OH Overlap

Figure 4 shows a visualization of a lifted transverse, methane jet flame at $r = 10$. The crossflow has been seeded with 0.1 μm glycerol fog particles which evaporate at approximately 150°C, illuminated by a thin pulsed light sheet from a Nd:YAG laser. Natural flame emission is exposed for 1/60 sec. The figure also outlines the approximate OH and PIV viewing regions at the lifted flame base. One can clearly see the entrainment of crossflow fluid into the jet upstream of the base of the lifted flame. The PIV viewing region (49.1 × 49.1 mm) includes the windward flame sheet in the center of the image, but shows only a small portion of the lee side flame sheet in the far upper left. The OH viewing region (97 × 65 mm) contains the entire PIV region so that it provides a larger-scale context for the velocity vectors; the penalty to signal for viewing such a large region is significant, but the present motivation for this diagnostic technique (i.e., measurement of strain or residence times in flame reaction zones) does not require large signal-to-noise ratio (SNR) in the OH images.

Before each run, a transparent ruled target suspended in the wind tunnel is imaged by each camera. Using two points from each of these target images, the pixel coordinates of each point are transformed to real space coordinates. The chosen transformation allows a scaling factor α (mm/pixel), x- and y-offsets (x_o, y_o), and a rotation angle θ to be determined from the registration points. The rotation correction for the PIV images was negligible ($\theta = 0.001$ radians rotation about center, equivalently 4 pixels ≈ 0.1mm from top to bottom), and hence was not performed, but the OH images were corrected for 0.0092 radians (0.53°) rotation. Uncertainty in the scaling factor α is about 1% in both images due to imperfect camera/target orthogonality, and this remaining uncertainty dominates the overall positional uncertainty of the pixels.

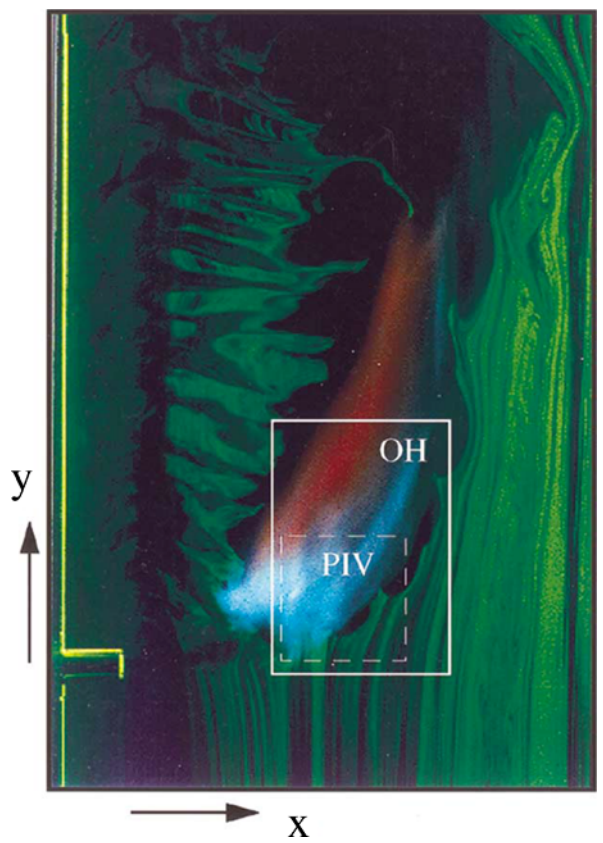

Fig. 4. An annotated photo of the transverse jet flame used in this study, showing approximate image regions for PIV (inner square) and OH PLIF (outer rectangle). The jet issues from the tube protruding into the wind tunnel at left into the upward crossflow. The jet exit inner diameter is about half the visible outer diameter due to the presence of an annular pilot tube around the main jet tube.

As mentioned in the introduction, several previous workers have inferred flame location using the density of particles in a PIV image without the benefit of simultaneous species measurements. Figure 5 shows a simultaneous PIV (Fig. 5a) and OH PLIF (Fig. 5b) image pair, and the overlaid results (Fig. 5c). As might be expected, the low particle density regions have a very high correlation with the presence of OH at the base of the flame. However, this correlation depends on uniform seeding of the jet and coflow. Streaks and other common nonuniformities in the flow seeding can cause some uncertainty, as shown for example in Fig. 6. Here there is low particle density in

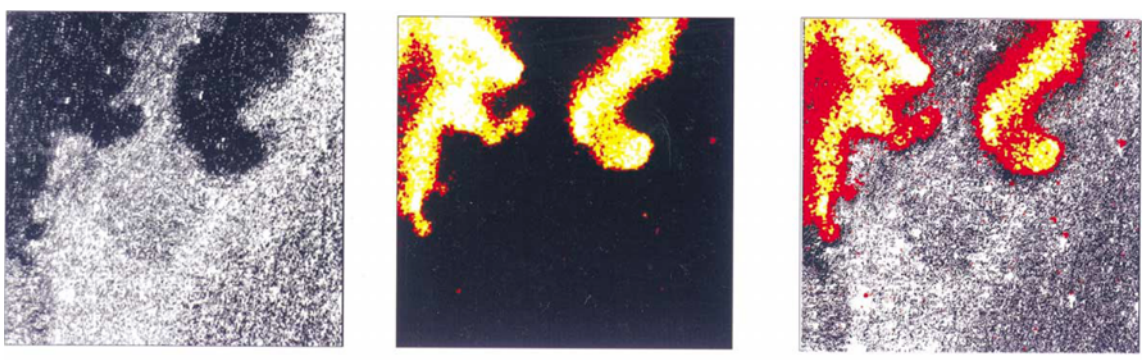

Fig. 5. (a) A typical PIV particle image, (b) Corresponding simultaneous OH image (c) An overlay of (a) and (b), demonstrating the validity of inferring flame location from particle density at the flame base.

some regions due to imperfect jet and crossflow seeding. An erroneous conclusion would be made by an automated system that the flame is present at the bottom of the image. A few of our 128 image pairs in this location showed seeding that could possibly mislead even human interpretation. However, with a simpler flow configuration and better seeding uniformity, the particle density can be relied upon as a marker of the flame base. On the other hand, nearer the flame tip, the smoother temperature gradients would certainly make particle density a less desirable diagnostic.

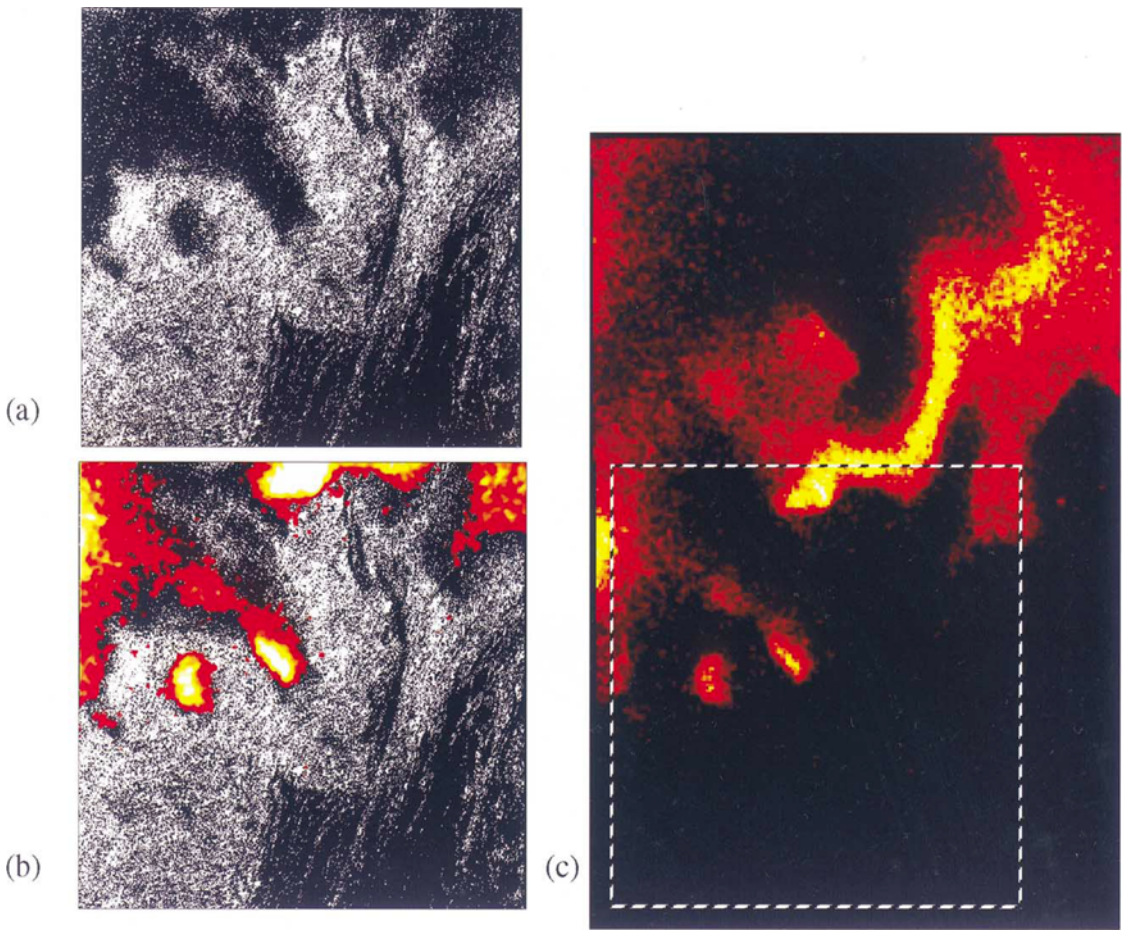

Fig. 6. (a) A particle image with nonuniform crossflow seeding, demonstrating possible difficulties in using only particles to determine the flamefront location in a complex flow. (b) The particle image with an OH image overlay, clearly showing that the lower right corner of (a) has low seeding density due to nonuniform seeding, not heat release (c) The full-field OH view, showing the PIV/OH overlap region in dashed lines. See Fig. 4 for the context of this window in the flow as a whole.

4.2 Flame Stabilization - Initial Results

Preliminary data obtained thus far demonstrate the important features of this flow, and how the flow and flame interact. Figure 7 shows a sample OH PLIF image (shown full viewing field) and its PIV velocity field counterpart (with only every third vector shown for clarity). It is possible to see that the transverse jet meanders about its mean trajectory, similar to the coflowing jet observations of Muñiz & Mungal (1996). Also, there is strong entrainment of crossflow fluid directly from the windward (front) side of the jet.

Figure 8 shows an overlay of velocity vectors and contours of velocity magnitude from another simultaneous image pair, with a heavy black contour outlining the OH zone. This figure clearly shows that the crossflow just upstream of the jet is deflected away from the jet and has been significantly slowed by the presence of the jet. The local jet width is about 3 cm, so it is not surprising that the local crossflow velocity should be

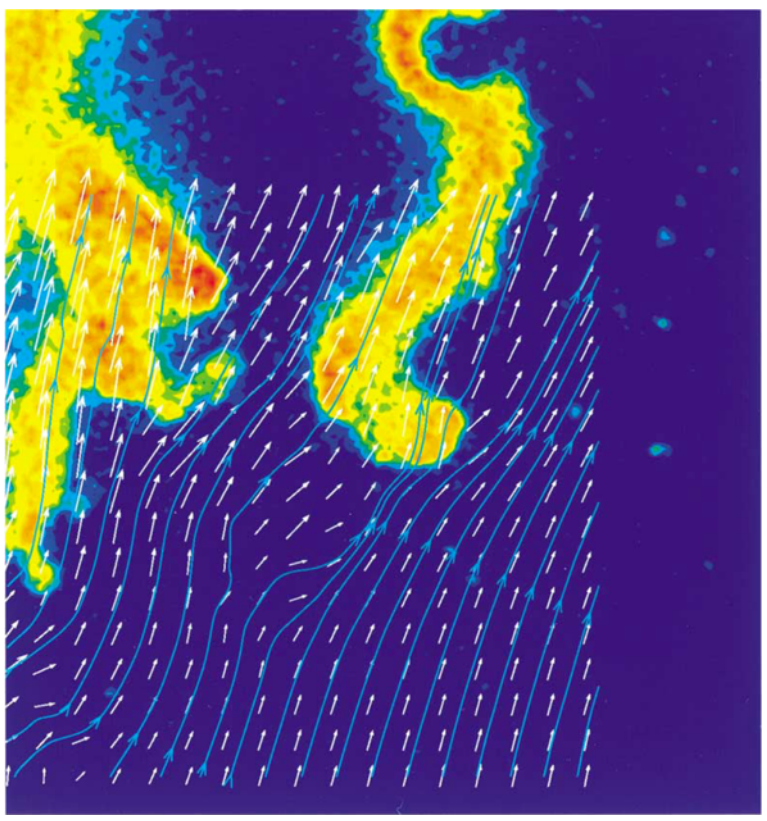

Fig. 7. A colormap of OH signal (blue to red) with vectors of the velocity field for one simultaneous PIV/OH PLIF image pair. Length of each arrowhead is proportional to the velocity magnitude. Only every third vector in each direction is shown for clarity. Streamlines are shown faintly in cyan.

affected over this distance. The velocity magnitudes in the lower-right corner are about 1.7 m/s, compared with 2.0 m/s without the jet.

Even lower velocity regions appear just upstream of the flame base, where the velocity magnitudes are about 1.3 m/s. This result is in agreement with the recent results of Muñiz & Mungal (1997), who have carried out PIV experiments in lifted coflowing jet flames of various compositions and coflow velocities. An analysis by Ruetsch et al. (1995) for partially premixed laminar triple flames suggests that the velocity (relative to the flame) at the flame base should be less than 2.7 times the laminar flame speed, S_L. Although we only measure the lab-frame fluid velocity, we typically find (as in this case) fluid velocity at the flame base near 3 S_L.

The flow accelerates sharply as it passes through the flame base to 5 m/s, about three times the local crossflow velocity upstream of the flame. The magnitude of the acceleration is also in agreement with the analysis of Ruetsch et al., and reflects the increase in velocity accompanying the decrease in density as the flow passes through the flame. Buoyancy plays a negligible role here, as the flow passes through the 1 cm acceleration zone in a few milliseconds.

We also point out that the OH zones observed here are quite thick, usually about 4 mm (full-width half maximum). This is significantly thicker than typical OH zones reported for attached, piloted undiluted methane diffusion flames, but are experimentally found for air-diluted flames according to Stårner et al. (1992). By comparison with strained-flame calculations, they argue that this broadening may be explained by a flame structure that is somewhere between purely diffusion flamelet and purely distributed. It therefore seems reasonable to conclude, along the same lines, that the flame base observed here is partially premixed.

There has been much debate over the nature of the leading edge of lifted jet flames, primarily over how to predict liftoff heights (Pitts, 1988). Much of the debate has been over whether the structure of the flame base can best be described as a fully turbulent premixed flame, or as a stretched nonpremixed laminar flamelet. However, the idea that the leading edge is best described as a partially premixed laminar flamlet has been gaining ground, (Peters, 1984), and it has even been suggested by Muñiz & Mungal (1996) and Schefer (1998) that the triple flame

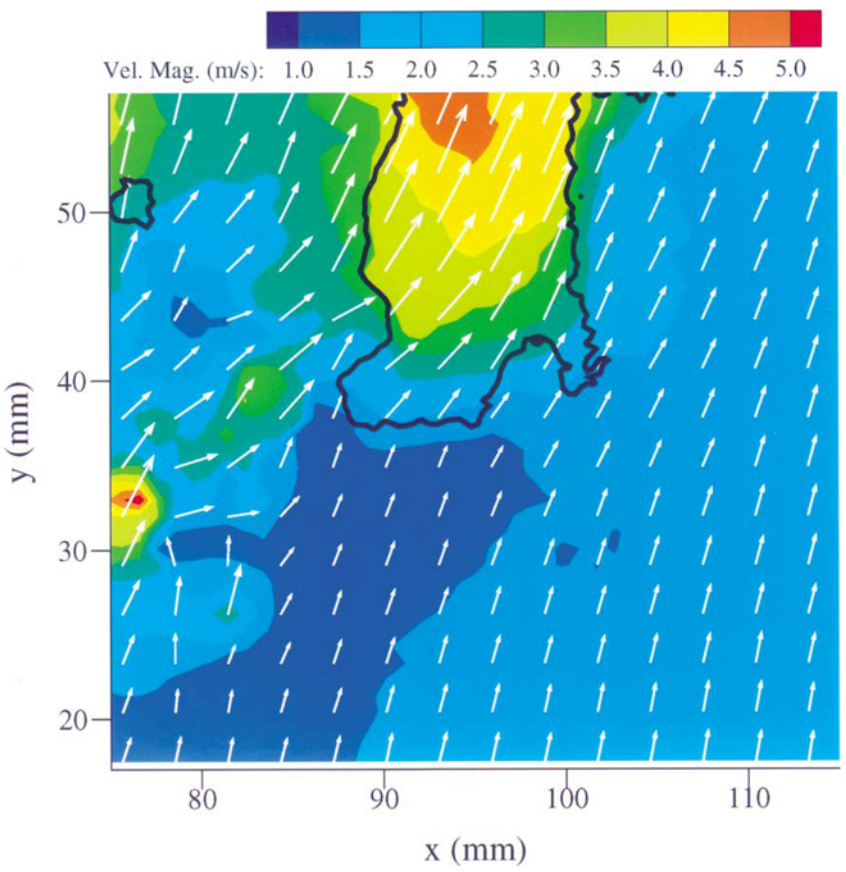

Fig. 8. A colormap of velocity magnitude, overlaid with the outline of high OH signal regions (heavy black line) and velocity field vectors. Of interest is the low velocity just upstream of the flame base, and the strong acceleration through the leading edge flame. Only every third vector is shown for clarity.

concept might be a candidate for flame base modeling. The present results suggest that the flame is at least partially premixed, that the flow decelerates just upstream of the leading edge of the flame, and that the fluid accelerates through the flamebase. Triple-flame-like structures in the OH distribution do not appear, however, as the turbulence distorts the leading edge significantly. However, it should be pointed out that the analysis by Ruetsch et al. (1995) strictly depends only on the existence of a finite-width partially premixed flame, not necessarily on a triple-flame structure. It appears that understanding partially premixed laminar flames, subjected to stretching and other complications, may be the key to understanding turbulent jet flame liftoff and blowout.

5. Discussion of the Technique

There are several possible improvements to the experimental setup presented here. The OH signal may be easily increased by reducing the size of the OH image region, to as low as unity magnification. Increased signal is also expected in hydrogen flames, which have 2.4 times higher equilibrium OH concentrations over methane flames. As discussed previously, there are some difficulties with quantitative OH imaging in the presence of particles. Semi-quantative images may be obtained by using the $Q_1(6)$ line and implementing shot-to-shot sheet corrections. Under most experimental situations, extinction of the PLIF laser sheet by particles (8% present case) should be less than the uncertainty presented by temperature and quenching (20%). It would be possible to correct for extinction using the PIV images, however extinction out of view of the imaged region has to be taken into account as well. In some experimental situations it may be possible to have a uniform cell of acetone in the imaged region for performing shot-to-shot sheet corrections.

As for the PIV portion of the technique, some redesign of the sychronization scheme would allow use of the PIV camera shutter, making it possible to eliminate the 532 nm line interference filter, increasing PIV signal by a factor of two. Our own future experiments will make use of an interline frame-transfer camera, capable of taking

two separate images at intervals as short as a microsecond. This will increase the dynamic range of the measurement since displacements less than a particle image diameter can be measured — a significant improvement, because the dynamic range of autocorrelation PIV is about 5 and the measured flow velocites range from 1 - 5 m/s. This will also allow us to reduce the time between laser pulses, reducing poor correlations due to out-of-plane motion.

Simultaneous OH PLIF with PIV also makes it possible to reduce PIV errors due to thermophoresis. Two-camera, two-line temperature measurements (Palmer & Hanson, 1990) would be ideal, but even single-shot OH PLIF images could be used along with equilibrium assumptions to provide a reasonable estimate of the temperature gradients and the required thermophoretic velocity correction. This is an issue for future work.

6. Conclusions

In general, preliminary results from simultaneous OH PLIF and PIV in turbulent flames show that the combined techniques provide a better, and potentially much more accurate, picture of flow/flame interaction than their independent application. However, there is significant room for improvement. Further investigation of the direct influence of the flame on the flow structure, and vice-versa, will continue along the lines presented here. Conclusions of the present work are:

- Nonresonant OH PLIF using the present scheme provides OH images with minimal interference due to the PIV particles. Out-of-plane fluorescence is less than 1% and particle influences on the flame are negligible.
- The primary contributor to PIV uncertainty in turbulent flames is thermophoresis, which can lead to errors up to 15 cm/s in velocity or about 150 s^{-1} in strain rate or vorticity. Simultaneous OH PLIF images may eventually provide a means for correcting most of this error.
- Particle density can be a viable indicator of flame front location if seeding density is uniform, temperature gradients are large, and the flow is relatively simple.
- The lifted transverse jet flame appears to be anchored in low-velocity regions of the flow, in agreement with recent observations by Muñiz & Mungal (1997). Strong accelerations of the fluid occur through the leading edge of the flame base. Most of the evidence supports the view of the leading edge flame to be a partially premixed flame.

Acknowledgments

The authors gratefully acknowledge the assistance of R. E. Martinez, L. Muniz, W. D. Urban, and T. C. Island. This work was supported by the Gas Research Institute, Contract No. 5093-260-2697, R. V. Serauskas, Technical Monitor. E. F. H. was partly supported by the Air Force Office of Scientific Research Laboratory Graduate Fellowship Program.

References

Adrian, R. J., Particle Imaging Techniques for Experimental Fluid Mechanics, Annual Reviews of Fluid Mechanics, 23(1991), 261.

Ashforth-Frost, S., et al., Comparison of interrogation methods for particle-image velocimetry, in Proceedings of SPIE - The International Society for Optical Engineering(1993), pp. 478-489, Publ. by Society of Photo-Optical Instrumentation Engineers, Bellingham, WA, USA.

Barlow, R. S. and Chen, J. Y., On transient flamelets and their relationship to turbulent methane-air jet flames, in Twenty-Fourth Symposium (International) on Combustion(1992), pp. 231-237, The Combustion Institute, Pittsburg, PA, USA.

Barlow, R. S. and Collignon, A., Linear LIF Measurements of OH in Nonpremixed Methane-Air Flames: When are Quenching Corrections Unnecessary, Twenty-Ninth Aerospace Sciences Meeting (Reno, NV), (1991), 91-0179.

Barlow, R. S., et al., Departure from Chemical Equilibrium in a Lifted Hydrogen Diffusion Flame, in 27th AIAA/ASME/SAE/ASEE Joint Propulsion Conference(Monterey), (1989), AIAA-89-0061.

Clemens, N. T. and Paul, P. H., Effects of heat release on the near field flow structure of hydrogen jet diffusion flames, Combustion and Flame, 102-3(1995), 271-284.

Dibble, R. W., et al., Resonance fluorescence imaging of CH in hydrocarbon flames using a polaroid filter to reject Rayleigh scattered light, in Proceedings of SPIE - The International Society for Optical Engineering(1990), Int. Soc. for Optical Engineering, Bellingham, WA, USA.

Drake, M. C. and Pitz, R. W., Comparison of Turbulent Diffusion Flame Measurements of OH by Planar Fluorescence and Saturated Fluorescence, Experiments in Fluids, 3(1985), 283-292.

Driscoll, J. F., et al., Strain exerted by a vortex on a flame - determined from velocity field images, Combustion Science and Technology, 96-4-6(1994), 213-229.

Frank, J. H., et al., Simultaneous Scalar/Velocity Field Measurements in Turbulent Gas-Phase Flows, Combustion and Flame, 107(1996), 1-12.

Gogineni, S., et al., Investigation of a Jet in a Crossflow Using PIV, AIAA 33rd Aerospace Sciences Meeting and Exhibit (Reno, NV), (1995), AIAA-95-0790.

Gomez, A. and Rosner, D. E., Thermophoretic effects on particles in counterflow laminar diffusion flames, Combustion Science and Technology, 89-5-6(1993), 335-362.

Hanson, R. K., et al., Planar laser-fluorescence imaging of combustion gases, Applied Physics B: Photophysics and Laser Chemistry, 50-6(1990),

441-454.
Hasselbrink, E. F., et al., Planar Velocity Measurements and OH Imaging in a Transverse Jet, 35th Aerospace Sciences Meeting and Exhibit (Reno, NV), (1997), AIAA-97-0118.
Johnson, A. W., et al., Thickness distribution of OH regions in a turbulent diffusion flame, Combustion Science and Technology, 89-1-4(1993), 1-7.
Kamel, M., et al., Simultaneous PLIF and Schlieren Imaging of Hypersonic Reactive Flows Around Blunted Cylinders, AIAA 35th Aerospace Sciences Meeting (Reno, NV), (1997), AIAA-97-0913.
Keane, R. D. and Adrian, R. J., Optimization of particle image velocimeters, part I: double-pulsed systems, Measurement Science and Technology, 1(1990), 1202-1215.
Lourenco, L. and Krothapalli, A., On the accuracy of velocity and vorticity measurements with PIV, Experiments in Fluids, 18-6(1995), 421-428.
Lourenco, L., et al., Particle Image Velocimetry, in Advances in Fluid Mechanics Measurement(1989), pp. 128-135, M. Gad-el-Hak, Editor. Springer-Verlag.
McMillin, B. K., et al., Comparison of NO and OH planar fluorescence temperature measurements in scramjet model flowfields, AIAA Journal, 32-10(1994), 1945-1952.
Mueller, C. J., et al., Effect of unsteady stretch rate on OH chemistry during a flame-vortex interaction: to assess flamelet models, Combustion and Flame, 100-1-2(1995), 323-331.
Mungal, M. G., et al., Instantaneous Velocity Measurements in Laminar and Turbulent Premixed Flames Using On-Line PIV, Combustion Science and Technology, 106(1995), 239-265.
Muñiz, L., et al., Application of PIV to Turbulent Reacting Flows, in Eighth International Symposium on Applications of Laser Techniques to Fluid Mechanics (Lisbon, Portugal), (1996).
Muñiz, L. and Mungal, M. G., Velocity Measurements in Lifted-Jet Diffusion Flames, in Western States Section Fall Meeting/The Combustion Institute (University of Southern California), (1996).
Muñiz, L. and Mungal, M. G., Instantaneous Flame-Stabilization Velocities in Lifted Jet Diffusion Flames, Combustion and Flame, 111-1/2 (1997), 16-31.
Palmer, J. L. and Hanson, R. K., Temperature imaging in a supersonic free jet of combustion gases with two-line OH fluorescence, Applied Optics, 35-Jan. 20(1996), 485-499.
Paul, P. H. and Dec, J. E., Imaging of reaction zones in hydrocarbon-air flames by use of planar laser-induced fluorescence of CH, Optics Letters, 19-13(1994), 998-1000.
Peters, N., Partially Premixed Diffusion Flamelets in Non-Premixed Turbulent Combustion, in Twentieth Symposium (International) on Combustion(1984), pp. 353-360, The Combustion Institute, Pittsburgh, PA.
Pitts, W. M., Assessment of Theories for the Behavior and Blowout of Lifted Turbulent Jet Diffusion Flames, in Twenty-Second Symposium (International) on Combustion(1988), pp. 809-816, The Combustion Institute, Pittsburgh.
Rehm, J. and Clemens, N. T., A PIV/PLIF Investigation of Turbulent Diffusion Flames, AIAA 35th Aerospace Sciences Meeting and Exhibit (Reno, NV), (1997), AIAA-97-0250.
Ruetsch, G., et al., Effects of Heat Release on Triple Flames, Physics of Fluids, 7-6(1995), 1447.
Schefer, R. W. and Goix, P. J., Mechanism of Flame Stabilization in Turbulent, Lifted-Jet Flames, Combustion and Flame, 112-4 (1998), 559-574.
Seitzman, J. M., Quantitative Applications of Fluorescence Imaging in Combustion, (1991), Ph.D. Thesis, Mechanical Engineering Department, Stanford University.
Seitzman, J. M. and Hanson, R. K., Comparison of excitation techniques for quantitative fluorescence imaging of reacting flows, AIAA Journal, 31-3(1993), 513-519.
Seitzman, J. M., et al., Imaging and Characterization of OH Structures in a Turbulent Nonpremixed Flame, in Twenty-Third Symposium (International) on Combustion(1990), pp. 637-644, The Combustion Institute.
Stårner, S. H., et al., Measurements of conserved scalars in turbulent diffusion flames, Combustion Science and Technology, 86-1-6(1992), 223-236.
Sung, C. J., et al., Thermophoretic Effects on Seeding Particles in LDV Measurements of Flames, Combustion Science and Technology, 99(1994), 119.
van de Hulst, H. C., Light Scattering by Small Particles (1981), Dover.
Westerweel, J., Analysis of PIV Interrogation with Low Pixel Resolution, in SPIE-2005 "Optical Diagnostics in Fluid and Thermal Flow" (San Diego, CA), (1993).